International Journal of Heat and Mass Transfer 51 (2008) 5623–5632

Contents lists available at ScienceDirect

International Journal of Heat and Mass Transfer

journal homepage: www.elsevier.com/locate/ijhmt

Water and solute active transport through human epidermis: Contribution of electromigration

Cibele V. Falkenberg [a], John G. Georgiadis [b,*]

[a] Beckman Institute of Science and Technology, University of Illinois at Urbana-Champaign, Urbana, IL 61801, USA
[b] Laboratory of Quantitative Visualization in Energetics, Department of Mechanical Science and Engineering, 140 Mechanical Engineering Building, 1206 W. Green Street, University of Illinois at Urbana-Champaign, Urbana, IL 61801, USA

ARTICLE INFO

Article history:
Received 15 January 2008
Received in revised form 4 April 2008
Available online 27 June 2008

Keywords:
Epidermis
Active transport
Ion pumps
Keratinocytes
Osmotic shock
Electromigration

ABSTRACT

A triphasic, coarse-grained model of mass transport through the human epidermis is developed, consisting of free extracellular water, live cells (keratinocytes), and inert extracellular matrix. The model accounts for the superposition of active transport of Na^+, K^+ and Cl^- ions across the membrane of keratinocytes, and electromigration driven by an externally imposed electrostatic potential difference. Local cell volume is regulated by the transmembrane fluxes of water and ions according to a time-delay scheme which aims to keep the volume between certain thresholds. Numerical simulations reveal that either weak hyposmotic shocks or negative potential gradients smaller than one millivolt/micrometer across the epidermis can generate travelling waves in extracellular ion concentration. By monitoring the transmembrane (Na^+–K^+ –ATPase) pump flux, we have found that maintaining a higher transepidermal potential gradient requires faster active transport through the cells.

1. Introduction

Skin is the largest organ of the body and it helps maintain homeostasis by establishing a chemical and biological barrier between the external environment and the vulnerable human cells. Understanding mass transfer through the skin is important for the clinician, engineer and scientist. More specifically, this understanding contributes to improving the treatment of wounds, the development of better clothes, the synthesis of benign skin care products, and the improvement of thermal comfort. Emerging applications include the control of transepidermal drug delivery through iontophoresis [1], development of tissue-engineered skin [2], and the formulation of treatments for obesity after elucidating the role of aquaporins [3]. Finally, understanding the permselectivity of skin might contribute to the development of bio-inspired ion exchange membranes for water purification [4].

The barrier function of the skin is related to its ultrastructure and physiology [5,6]. Human skin is a complex, multilayered tissue comprising approximately 2 m^2 of body surface and contributing approximately 16% of the body weight of the average adult. The outermost layer of the viable skin, the epidermis, is a constantly renewed stratifying squamous epithelium, varying in thickness from about 50–800 μm, cf. Fig. 1. The basal cells of the epidermis (*stratum basale*) proliferate and differentiate as they migrate outwards. Initially columnar, these epidermal cells (keratinocytes) become rounded, and finally flatten out and die (apoptosis) as they migrate to the outer layer, the *stratum corneum*. This outmost layer is less permeable than the viable layer and its thickness is sensitive to hydration level variation [6]. Below the epidermis and delineated by the corrugated basal membrane lies the dermis, a highly vascular connective tissue tethered by collagen fibers to the subcutaneous areas of the skin which is cushioned by adipose tissue. The contribution of sweat glands and hair to transepidermal transport is outside the scope of this investigation.

The epidermis forms the primary barrier to mass transfer. Its viability relies on bulk diffusion of water and nutrients since it is devoid of any blood circulation. Prior mass transport studies focused only on the *stratum corneum* which consists of dead cells, and did not consider the deeper layers of the epidermis. In steady state, the *stratum corneum* has been modelled as a passive barrier of constant (effective) conductance. For example, Kalia et al. [7] fit the transepidermal transport data obtained after consecutive tape stripping to Fickian diffusion models. Such empirical models fail to reproduce the increase of permeability with hydration. Kasting et al. [8] developed a more sophisticated model employing a concentration-dependent diffusivity for water to reconcile theory with experiments.

Ion migration through the skin is ultimately related to an electrostatic potential across the skin, with the skin surface being more negative than the inner layers. There exist very few investigations of this interplay owing to the difficulty of measuring ion concen-

* Corresponding author.
E-mail address: georgia@uiuc.edu (J.G. Georgiadis).

0017-9310/$ - see front matter © 2008 Elsevier Ltd. All rights reserved.
doi:10.1016/j.ijheatmasstransfer.2008.04.047

Nomenclature

A_c	area of cell membrane
c_i	molar concentration of ion i
$\mathbf{D}^*_{mi}$	effective transport coefficient
$\mathbf{D}^{**}$	effective total transport coefficient
F	Faraday constant
J_i	transmembrane flux of ion i, or net ionic pump flux when $i = p$
j^*_i	molar flux of ion i
m_i	number of moles of ion i
P_i	membrane permeability for ion i
Q^*_K	constant for volume induced transmembrane flux, due to KCl cotransporter
Q^*_{Na}	constant for volume induced transmembrane flux, due to NaCl cotransporter
R	universal gas constant
S_{ij}	source term of ion i in phase j
T	temperature
v^+	upper threshold for cell volume
v^-	lower threshold for cell volume
$\mathbf{v}^*_i$	molar velocity vector of phase i
V_m	cell membrane potential
V_c	cell volume
t	time
x	spatial coordinate normal to epidermis
X^-	membrane-impermeable extracellular species with valence -1
z_i	valence of ion i

Greek symbols

Δ	difference operator
ε_o	permittivity of free space
ε	dielectric constant of water
θ_i	volume fraction of phase i
τ	time delay
ϕ_K	transmembrane flux due to KCl cotransporter
ϕ_{Na}	transmembrane flux due to NaCl cotransporter
ψ	electrical potential

Subscripts

i	ionic species
j	phase
α	extracellular fluid phase
β	intracellular fluid phase
γ	extracellular solid phase

tration profiles in the epidermis [9]. In addition to its relevance in iontophoresis, the skin surface electric potential has been widely used for physiological or psychological studies but the mechanism of its generation has not been elucidated. Denda et al. [10] investigated experimentally the interplay between epidermal ion concentration and endogenous skin surface potential in hairless mice skin in organ culture, and suggested that the ion flux through the keratinocyte membrane regulates this potential.

To fill several gaps in the area of physiologically-motivated models of transport through live tissue, the present study focuses on the transport of water and several ionic species across the viable part of the epidermis which is devoid of a *stratum corneum* layer. Water and ion transport through any viable tissue involves transcellular as well as paracellular pathways. Therefore, candidate mass transport models have to account for both local extracellular transport and transmembrane fluxes, the later coupled to cell volume regulation. Fifty years before high resolution images of ion transmembrane channels became available, their role was modeled by the Goldman–Hodgkin–Katz equation, which has been used to correlate intracellular and extracellular concentrations, permeabilities, and membrane potential [11]. Even water transport across cellular membranes is not fully understood. A process of solute–water cotransport is proposed as a possibility, against the so far accepted osmotic transport mechanism [12]. Adding to the multitude of pumps and ion channels, a number of cotransporters coexist in the cell membranes [11]. Animal cell regulation has not been fully described mathematically, since the activation and regulation mechanisms of each independent pathways are not completely known. As a tool to investigate the effects of live cells on mass transport in a tissue, the simplified model proposed by Hernández and Cristina [13] is chosen for the present study. This generic model accounts for the basic components of cell volume regulation, which includes the function of ion channels for sodium, potassium and chloride, the sodium potassium pump, and cotransporters which are activated under stress conditions. As more sophisticated and tissue specific models become available, the various components of the compound model can be simply substituted for the simplified model.

In anticipation of the ultimately integration of water and ion concentration measurements obtained with novel techniques [14,9] towards explaining the barrier function of the whole epidermis, a realistic model of the tissue as an active, rather than a passive, medium is needed. The emphasis of the present study is to characterize the contribution of electromigration. Specifically, we aim to model the variation of interstitial (extracellular) water and the concentration of three physiologically-relevant solutes (Na^+, K^+ and Cl^- ions) through the viable non-swelling epidermis due to an imposed (exogenous) electric potential difference across the epidermis. We proceed in two steps: first, we develop a polyphasic model including active transport of the three ions through the membrane of the keratinocytes, and second, we use the model to predict of response of the epidermis to osmotic shocks and electrostatic gradient effects.

2. Formulation of polyphasic model for epidermis

The viable epidermis is modeled as a volume-averaged porous medium with three distinct phases: the extracellular fluid phase, denoted by α, the intracellular fluid phase, denoted by β, and the extracellular matrix, denoted by γ. The extracellular fluid phase α contains water, Na^+, K^+ and Cl^- ions, and larger, less mobile molecules which are dissolved in water. The cell membrane is not permeable to these larger molecules, which have a valence of -1 and are collectively referred as component X^- in the model discussed below. The phase β contains water and the same three ions, and all non-water-soluble chemicals are assigned to the γ phase. This decomposition in three phases allows a coarse-grained representation of the tissue. The spatial characteristic scale in the model is larger than the representative elementary volume (REV), which in turn is larger than the scale of a single epidermal cell, as shown in Fig. 2. Given the thickness of the epidermis (x-direction), and in order to maintain separation of spatial scales, the REV is defined as a long prism with its principal axis perpendicular to the x–y plane. The x-coordinate defines the direction normal to the skin and pointing towards the ambient air, while the y-coordinate is tangential to the skin surface. The modeling of each of the three phases is discussed below.

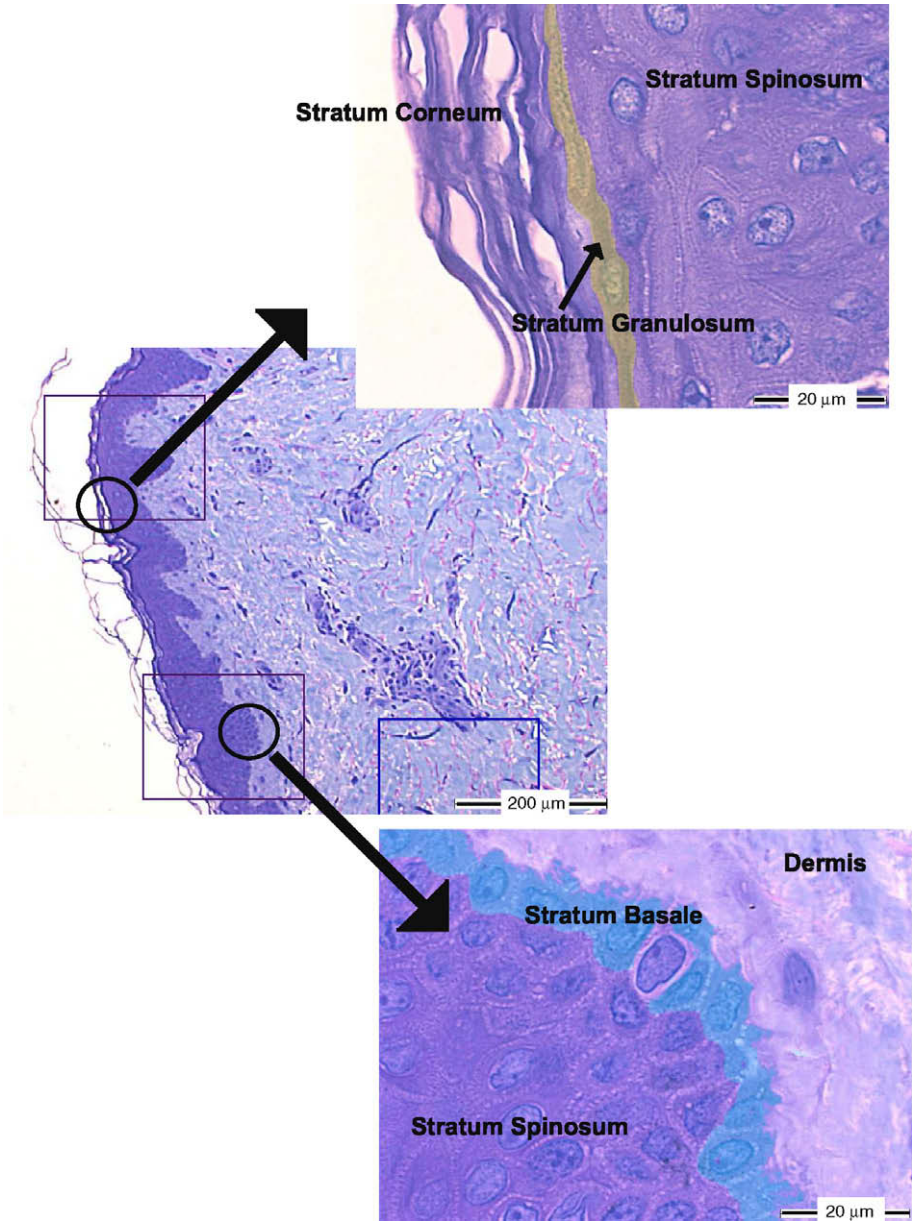

Fig. 1. Stained cross-sections of human epidermis (thin skin), courtesy of the UIUC internet Atlas of histology.

2.1. Active transport through keratinocytes

The β phase consists of keratinocytes. Each cell volume is regulated by osmosis and any osmotic imbalance is corrected by passive and active ion exchange across the cell membrane. Potassium, chloride and sodium ions are transported through specialized ion channels. The sodium–potassium pump ($Na^+ - K^+$ −ATPase) uses energy from ATP oxidation to transport ions against the concentration gradient, keeping the intracellular fluid at high K^+ and low Na^+ concentrations. To represent active cell volume regulation we adopt the model proposed by Hernández and Cristina [13] which is based on five assumptions: (a) the cells are non-polarized; (b) all cell volume changes are caused by water movement across the membrane; (c) the stoichiometric pump ratio $3Na^+ : 2K^+$ is fixed; (d) the cell volume decrease is mediated by coupling the fluxes of K^+ and Cl^-, and the volume increase by Na^+ and Cl^- fluxes; (e) constant cell surface area A_c available for water transport. Assumption (d) pertains to the restoration of the individual cell to its physiological state. It involves the introduction

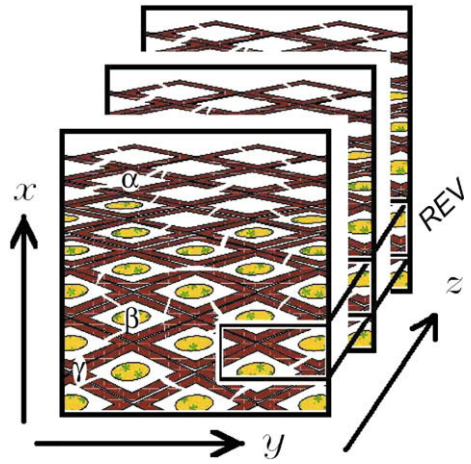

Fig. 2. Representative elementary volume (REV) used for volume averaging in the epidermis.

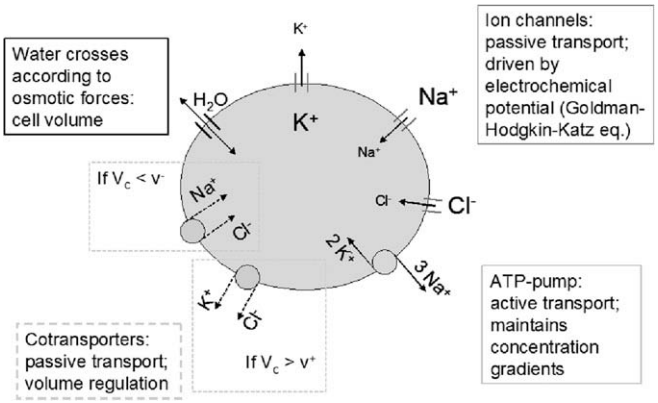

Fig. 3. Pathways used in modeling cell volume regulation.

of two volume threshold values, v^+ and v^-, which trigger a net KCl efflux and NaCl influx, respectively. The model uses only the above mentioned cotransporters as representatives of the plethora of cotransporters involved in cell volume regulation.

The key equations of the model [13] are listed below, while a graphical representation of the various cell regulation mechanisms is portrayed in Fig. 3. The inward transmembrane ion fluxes J_i through ion channels on the cell membrane follow the Goldman–Hodgkin–Katz current equation,

$$J_i = P_i \frac{z_i F V_m}{RT} \frac{\langle c_{i\alpha}\rangle^{\alpha} - \left(\frac{m_i}{V_c}\right) e^{\frac{z_i F V_m}{RT}}}{e^{\frac{z_i F V_m}{RT}} - 1}. \tag{1}$$

The intracellular ion concentrations and the cell volume obey the following ordinary differential equations:

$$\frac{d(m_{Na})}{dt} = A_c(-3J_p + J_{Na} + \phi_{Na}), \tag{2}$$

$$\frac{d(m_K)}{dt} = A_c(2J_p + J_K + \phi_K), \tag{3}$$

$$\frac{d(m_{Cl})}{dt} = A_c(J_{Cl} + \phi_{Na} + \phi_K), \tag{4}$$

$$\frac{d(V_c)}{dt} = A_c V_w P_w \sum_i \left(\frac{m_i}{V_c} - \langle c_{i\alpha}\rangle^{\alpha}\right). \tag{5}$$

Intracellular electroneutrality is maintained by the sodium–potassium pump, represented by the flux J_P in Eqs. (2) and (3). The intracellular molar concentrations are represented by the ratio m_i/V_c, where V_c is the cell volume. The term $\langle c_{i\alpha}\rangle^{\alpha}$ representing the extracellular molar concentrations is introduced systematically later, in the context of the volume averaging scheme. The fluxes due to cotransporters are represented by the terms ϕ_{Na} and ϕ_K, which are functions of cellular and extracellular concentrations of Na^+ and Cl^-, and K^+ and Cl^-, respectively. While the cell volume remains between the two specified threshold values v^- and v^+, i.e. while $v^- < V_c < v^+$, the induced fluxes ϕ_{Na} and ϕ_K are null. Whenever the cell volume falls outside the threshold range, and after a predetermined time delay τ, an appropriate volume-induced ion flux (ϕ_{Na} for $V_c < v^-$ and ϕ_K for $V_c > v^+$) is generated according to the equation below:

$$\phi_{Na,K} = -Q^*_{Na,K}\left|\frac{v^{-,+} - V_c}{v^{-,+}}\right|\left(\langle c_{Na,K_\alpha}\rangle^{\alpha}\langle c_{Cl_\alpha}\rangle^{\alpha} - \frac{m_{Na,K}}{V_c}\frac{m_{Cl}}{V_c}\right). \tag{6}$$

The membrane potential is related to various cell parameters via the following algebraic equation:

$$V_m = \frac{RT}{F}\ln(\kappa). \tag{7}$$

The argument κ represents various functions of intracellular and extracellular ionic concentrations, membrane permeabilities, $Na^+ - K^+ -$ ATPase membrane density, and the rate constants associated with the transmembrane pumps. The functional form of the variable κ is presented below,

$$\begin{aligned}
\kappa &= \frac{k_c + f_{c1}}{\mu_c + f_{c2}}\\
k_c &= \left(P_{Na}\langle c_{Na_\alpha}\rangle^{\alpha} + P_K\langle c_{K_\alpha}\rangle^{\alpha} + P_{Cl}\frac{m_{Cl}}{V_c}\right)f_{c3}\\
\mu_c &= \left(P_{Na}\frac{m_{Na}}{V_c} + P_K\frac{m_K}{V_c} + P_{Cl}\langle c_{Cl_\alpha}\rangle^{\alpha}\right)f_{c3}\\
f_{c3} &= \left(\frac{FV_m}{RT}\right)\frac{e^{\left(\frac{FV_m}{2RT}\right)}}{\left(e^{\left(\frac{FV_m}{RT}\right)} - 1\right)}
\end{aligned} \tag{8}$$

The functions f_{c1} and f_{c2} represent the sodium–potassium pump cycle, and are dependent on intracellular and extracellular concentrations of the ions Na^+ and K^+ and concentrations of ATP and ADP. More details can be found in Hernández et al. [15].

2.2. Volume-averaged transport equations

The mathematical formulation of transport in phases α and β hinges on the development of generic porous medium models, as described in Bear and Buchlin [16]. In the following, subscripts denote the phase j, angle brackets $\langle\cdot\rangle$ denote *volumetric phase averages*, and $\langle\cdot\rangle^j$ denotes the corresponding *intrinsic volumetric phase averages* over a given phase j. The ratio of the two averages defines the volumetric fraction θ_j, which represents the fraction of the total volume occupied by phase j. Each phase is considered incompressible and the exchange of matter between phases is accounted for by a source term $\langle S_j\rangle$ in the conservation equation for each phase j, as follows:

$$\frac{\partial\langle c_j\rangle}{\partial t} + \nabla\cdot\langle c_j\mathbf{v}^*_j\rangle = \langle S_j\rangle \quad j = \alpha,\beta,\gamma. \tag{9}$$

The molar velocity of j phase is expressed by $\mathbf{v}^*_j$. By expanding the concentration into a product of volume fraction of the phase and the intrinsic concentration of each phase, and assuming that both phases α and β constitute dilute solutions, it is convenient to rewrite Eq. (9) as

$$\frac{\partial\theta_j}{\partial t} + \nabla\cdot\left(\theta_j\langle\mathbf{v}^*_j\rangle^j + \frac{\langle\dot{c}_j\dot{\mathbf{v}}^*_j\rangle}{\langle c_j\rangle^j}\right) = \frac{\langle S_j\rangle}{\langle c_j\rangle^j}. \tag{10}$$

The numerator on the third term represents hydrodynamic dispersion. It consists of the product of deviations of local concentration $\dot{c}_j$ and molar velocity $\dot{\mathbf{v}}^*_j$ from its local average value, and it can be neglected for the bulk phases.

It is known that epidermal cells migrate outwards with a time scale on the order of days, which is much slower than the time scale for diffusive transport in the extracellular fluid phase. The extracellular matrix for the viable epidermis is assumed to be inert (not exchanging ions or solvent), and does not shrink or swell due to water and ion transport through the viable layer. As a consequence, the molar velocities $\mathbf{v}^*_\beta$ and $\mathbf{v}^*_\gamma$ are null and the local volume fraction of the solid phase, θ_γ, is constant in time. Since no chemical reactions are taken into account in any of the phases, the sum of source terms is zero. In the viable epidermis, the use of Eq. (10) for the intracellular phase reveals that the source term corresponds to a local change in volume fraction of the β-phase. The equation for velocity of the extracellular fluid phase can be obtained from Eq. (10):

$$\nabla\cdot(\theta_\alpha\langle\mathbf{v}^*_\alpha\rangle^{\alpha}) = 0. \tag{11}$$

Similarly, the evolution equation governing the average concentration c_i of each solute i in the composite medium can be obtained by volume-averaging the mass conservation equation for each solute over the representative elementary volume:

$$\sum_j \frac{\partial(\theta_j\langle c_{ij}\rangle^j)}{\partial t} = -\sum_j \nabla\cdot(\theta_j\langle \mathbf{j}^*_{ij}\rangle^j) - \sum_j \nabla\cdot\langle c_{ij}\mathbf{v}^*_j\rangle, \quad j=\alpha,\beta,\gamma. \tag{12}$$

When two subscripts are used, henceforth, the first denotes the ion and the second the phase. Two models for the average diffusive flux will be considered here. The first corresponds to neutral solutes and the second to charged solutes (ions). The choice of which model is appropriate for our case depends on whether electrokinetic flux is significant. Neglecting bulk molar concentration variations, the average diffusive molar flux $\mathbf{j}^*$ for the first case is given by the Fickian constitutive equation

$$\langle \mathbf{j}^*_{ij}\rangle^j \equiv -\mathbf{D}^*_{mi}\nabla\langle c_{ij}\rangle^j, \tag{13}$$

where $\mathbf{D}^*_{mi}$ is the effective transport coefficient, which is different from the molecular diffusion coefficient D because the former accounts for the diffusion over the complex extracellular space.

Combining the coefficients of molar diffusion and dispersion (the latter emerging from the last term of Eq. (12)) into an effective total transport coefficient $\mathbf{D}^{**}$, the governing equation for solute transport through the composite medium representing the viable epidermis is obtained from a combination of Eqs. (12-13):

$$\begin{aligned}&\frac{\partial\theta_\alpha}{\partial t}\langle c_{i\alpha}\rangle^\alpha + \frac{\partial\langle c_{i\alpha}\rangle^\alpha}{\partial t}\theta_\alpha + \frac{\partial\theta_\beta}{\partial t}\langle c_{i\beta}\rangle^\beta + \frac{\partial\langle c_{i\beta}\rangle^\beta}{\partial t}\theta_\beta \\ &\quad = +\nabla\theta_\alpha\cdot(\mathbf{D}^{**}\nabla\langle c_{i\alpha}\rangle^\alpha - \langle c^\alpha_{i\alpha}\rangle\langle\mathbf{v}^*_\alpha\rangle^\alpha) + \theta_\alpha\nabla\cdot(\mathbf{D}^{**}\nabla\langle c_{i\alpha}\rangle^\alpha \\ &\qquad - \langle c_{i\alpha}\rangle^\alpha\langle\mathbf{v}^*_\alpha\rangle^\alpha).\end{aligned} \tag{14}$$

Note that there are no transport terms intrinsic to the β phase. Such simplification is justified by discontinuity of such phase and slower mass transport across the cellular membrane than in the intracellular phase. The terms pertaining to the extracellular matrix vanish since phase γ is assumed to be incompressible and does not exchange mass with the rest. The intracellular values for concentration and volume fraction are given as a function of time by integrating the active keratinocyte model discussed in the previous section, so that Eq. (14) can be integrated for the concentrations of each ion i in α phase, given the absolute velocity $\langle\mathbf{v}^*_\alpha\rangle^\alpha$. The above model is strictly valid for non-charged solutes in dilute solutions.

2.3. Electromigration flux

In the case of charged solutes exposed to an electrical field, an additional solute flux is generated. The flux in Eq. (13) needs to be augmented by the addition of the electromigration flux to yield the Nernst–Planck equation [17,18]:

$$\mathbf{j}^*_i = -\mathbf{D}\left(\nabla c_i + \frac{z_i F c_i}{RT}\nabla\psi\right). \tag{15}$$

By analogy to the Fickian diffusion problem, volume-averaging the second term on the right hand side of Eq. (15) gives the following expression for the average electrokinetic flux,

$$\langle \mathbf{j}^*_{e,ij}\rangle^j \equiv -\frac{z_i F}{RT}\mathbf{D}^{**}\langle c_{ij}\rangle^j\nabla\langle\psi\rangle. \tag{16}$$

In general, the electrical potential ψ is given by invoking classical electrostatics:

$$\nabla^2\langle\psi_\alpha\rangle^\alpha = -\frac{F}{\varepsilon\varepsilon_o}\sum\langle c_{i\alpha}\rangle^\alpha z_i. \tag{17}$$

When extracellular electroneutrality is violated, the right-hand side of (17) is not negligible, but the model becomes very complex, since the Poisson Eq. (17) has to be solved coupled with Eqs. (12) and (15). Fortunately, electromigration caused by deviations of electroneutrality due to the small differences in solute diffusion coefficients is negligible [17,19], so (17) reduces to Laplace's equation. However, the electromigration flux is not negligible in the case of externally imposed static electric field, as it will be shown in the next section.

3. Results

3.1. Physical and numerical parameters

The living epidermis has a thickness between 30 μm and 130 μm, and features the highest water content in the skin, ranging from more than 70% (in the basement membrane) to 15% (top of the stratum corneum layer). For the current investigation we consider a stratified medium confined in a homogeneous layer and limit the model to transport in one dimension, x (normal to the epidermis), since it is the direction of greater gradients, while volume averaging occurs in the y–z plane, as shown in Fig. 2. For definiteness, we consider initial volume fractions $\theta_\alpha = 0.2$, $\theta_\beta = 0.4$ and $\theta_\gamma = 0.4$, and a tissue thickness of 60 μm and 100 μm, with a trans-epidermal profile that is initially uniform in space.

Most of the parameters used for cell regulation are taken from [13]. The reference (initial) condition for extracellular concentrations are $\langle c_{Na\alpha}\rangle^\alpha = 14\times10^{-5}$ mol/cm³, $\langle c_{K\alpha}\rangle^\alpha = 1\times10^{-5}$ mol/cm³, $\langle c_{Cl\alpha}\rangle^\alpha = 14\times10^{-5}$ mol/cm³, $\langle c_{X\alpha}\rangle^\alpha = 1\times10^{-5}$ mol/cm³. Intracellular concentrations are $\langle c_{Na\beta}\rangle^\beta = 1.84\times10^{-5}$ mol/cm³, $\langle c_{K\beta}\rangle^\beta = 13.20\times10^{-5}$ mol/cm³, $\langle c_{Cl\beta}\rangle^\beta = 3.02\times10^{-5}$ mol/cm³, $\langle c_{X\alpha}\rangle^\alpha = 18.00\times10^{-5}$ mol/cm³. The membrane permeabilities for Na^+, K^+ and Cl^- are $10^{-7}, 5\times10^{-7}$ and 10^{-6} cm/s, respectively, while the water permeability is $P_w = 1.5\times10^{-2}$ cm/s. We should note in passing that the ratio between water and ion channel permeability, P_w/P_i, is of order 10^5. Since transcellular ion transport is much slower than that for water, the cells act as ion point sinks or sources.

The corresponding resting membrane potential (defined as intracellular minus extracellular potential) is $V_m = -41$ mV. We fix the time delay to $\tau = 10$ s and the magnitude of the coefficients for the induced fluxes to $Q^*_{Na} = 0.1$ cm⁴/(mols) and $Q^*_K = 10$ cm⁴/(mols). The volume and area of the cell are modified so that the geometry of the cell represents the keratinocytes. The approximate diameter for the cells is 10 μm [20], and the corresponding cubical cell has volume 10^{-9} cm³ and surface area 6×10^{-6} cm². The model assumes constant area for the cellular membrane and in order to accommodate the 5% increase in cell volume, the fixed surface area becomes $A_c = 6.2\times10^{-6}$ cm². It is assumed that half of the cell volume is available for the cytoplasmic fluid, so $V_c = 5\times10^{-10}$ cm³.

The molecular diffusion coefficients are $D_{Na} = 2.03\times10^{-9}$ m²/s, $D_K = 1.38\times10^{-9}$ m²/s, $D_{Cl} = 2.11\times10^{-9}$ m²/s, and the fourth solute X^-, which does not permeate across the cell membrane, is assigned a molecular diffusion coefficient of $D_X = 10^{-11}$ m²/s. We finally need to prescribe the dependence of the extracellular dispersion coefficient with the volume fraction of phase α. Assuming a homogeneous 'brick and mortar' wall-like distribution of keratinocytes, the following expression for the ratio $\Lambda^2 = D/D^{**}$ is obtained from a correlation we developed based on the results of Chen and Nicholson [21]

$$\Lambda = 2.28156 - 5.21948\ \theta_\alpha + 15.6529\ \theta^2_\alpha - 19.1835\ \theta^3_\alpha + 7.46849\ \theta^4_\alpha \tag{18}$$

The transcellular transport Eqs. (2)–(5) are four first-order ordinary differential equations and are integrated using a fourth-order Runge–Kutta method. Our numerical scheme was validated by comparing its predictions with the single cell case [13]. The extracellular transport model consists of three advection-diffusive-reactive partial differential Eq. (14), along with the contribution of (16)

in the case of electromigration, which are integrated using finite-difference discretization via a third-order implicit Adam's method (including a three nodes upwind scheme). After temporal and spatial convergence of the numerical scheme was verified [22], the numerical time step was set at 5×10^{-4} seconds and a uniform mesh with 101 nodes was used in the x direction.

3.2. Externally imposed osmotic shocks

Hyposmotic/hyperosmotic shocks are imposed at the lower (basal) boundary ($x = 0$) by decreasing/increasing extracellular concentrations of Na^+ and Cl^-, while imposing zero ionic flux at the upper (appical) boundary ($x = 100\ \mu m$). The time delay in cell regulation is set to $\tau = 10$ s. The change in concentration at the lower boundary is introduced as a ramp of 5 s duration with a total decrease/increase of the two species concentrations corresponding to 10% of the initial values. Subsequently, the concentrations on the lower boundary are kept constant for the remaining time of the simulation. The osmotic shock is imposed in such a way that both species have equal concentrations at all times at the lower boundary and electroneutrality is locally maintained.

We focus here on the response of the epidermis to a hyposmotic shock. The extracellular concentrations of Na^+ and Cl^- undergo a 10% decrease by ramping to the final value within 5 s, and are maintained fixed at that value for the remaining simulation time. Fig. 4 shows the response of the extracellular volume fraction as a function of space and time. After an initial undershoot and within a minute from the imposition of the shock, a train of propagating waves appears, with amplitudes that decay in time. The initial undershoot in extracellular volume fraction coincides with an overshoot of cellular volume (not shown here), which is a result of extracellular water flowing into the cell to compensate for higher internal salinity. The extracellular ion concentrations exhibit similar propagating waves which coincide in wavelength with that of the extracellular volume fraction, as seen in Fig. 5 for Na^+.

Having performed analogous simulations for hyperosmotic shocks (reported in [22]), we have found that only in the case of the hyposmotic shock is the initial undershoot of extracellular volume followed by a series of propagating waves, starting from the basal side of the layer ($x = 0\ \mu m$) where the shock is initially imposed. This result is consistent with the observations from the single cell response in an infinite medium. We hypothesize that these waves are caused by the delayed (by $\tau = 10$ s) activation of the cell membrane cotransporters introduced in the model of Hernández and Cristina [13], in conjunction with the high value of the constant Q^*_K for volume-induced flux given by Eq. (6). Our hypothesis is motivated by the observation that the amplitude of the volume-induced flux of the K^+ ion is larger than that for the Na^+ ion by two orders of magnitude ($Q^*_K \gg Q^*_{Na}$). We have shown [22] that for smaller values of Q^*_K, the undershoot and periodic waves vanish. The existence of wave-like solutions of the model formulated here is characteristic of excitable reaction–diffusion systems [23], but this constitutes a problem whose mathematical nuances need to be addressed in the future.

3.3. Shocks induced by electrostatic potential difference

By a scaling analysis of Eqs. (13) and (16), we can estimate the magnitude of the potential difference that is required across the epidermis so that the induced ion flux (electromigration) becomes comparable to the diffusive flux:

$$\Delta\psi = O\left(\frac{RT}{z_i F}\frac{\Delta c_i}{c_i}\frac{\Delta x_\psi}{\Delta x_c}\right). \tag{19}$$

For a normal physiological temperature $T = 310\ K$, the above yields

$$\Delta\psi = 26.7\ \frac{\Delta c_i}{c_i}\ \text{mV} \tag{20}$$

Assuming that the electrostatic and concentration profiles have equivalent length scales ($\Delta x_\psi \simeq \Delta x_c$), Eq. (20) implies that an external potential difference of $\Delta\psi = -2.67$ mV would induce a concentration difference (Δc_i) that is 10% of c_i. This potential difference is indeed very small. For comparison, the well known drug delivery method of iontophoresis uses a potential on the order of 1 V, but it is more likely that at such voltages, the transport conduits include large pores in the epidermis [24].

In order to study the interaction between electromigration in a viable tissue and the cell regulation mechanisms, the following

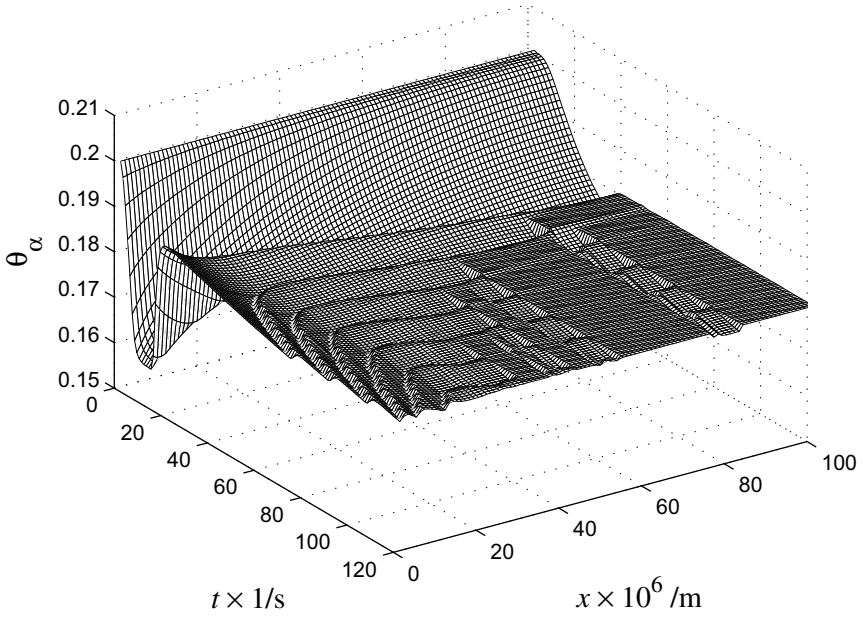

Fig. 4. Viable epidermis response to hyposmotic shock. Spatio-temporal variation of extracellular volume fraction following a 10% decrease of Na^+ and Cl^- concentrations at the basal surface of the epidermis ($x = 0$).

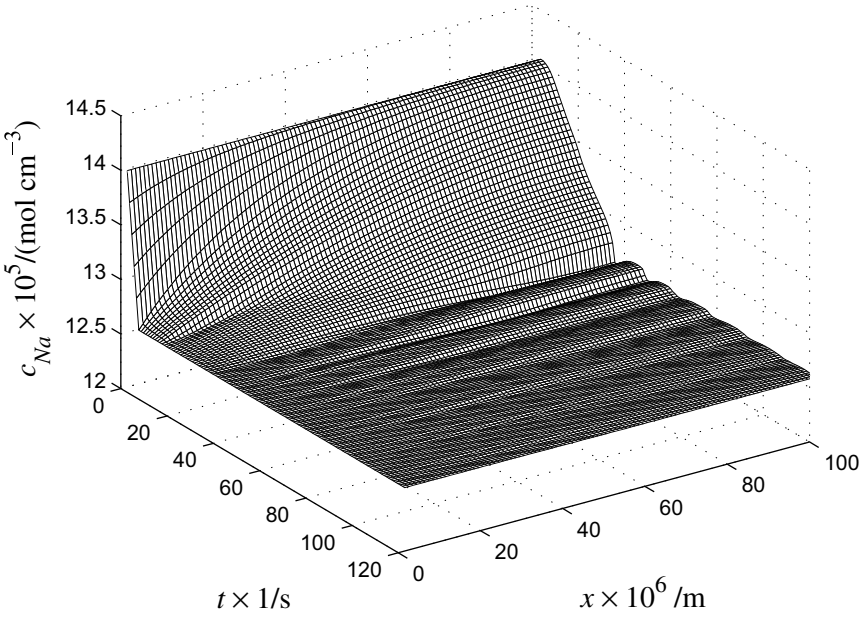

Fig. 5. Variation of extracellular Na^+ concentration for 10% decrease of Na^+ and Cl^- concentrations at $x = 0$.

simulations are performed. At time $t = 0$, a linear electric potential profile is imposed between the boundaries $x = 0$ and $x = 60$ μm, with the outer boundary ($x = 60$ μm) more negative than the inner. This profile satisfies Laplace's equation. The numerical simulation is repeated for three potential differences across the layer, chosen to be 1, 2 and 5 times the value −2.67 mV. Ion concentration gradients are generated as a result of diffusion and electromigration fluxes. The effect of imposing a potential difference of $\Delta\psi = -13.35$ mV (the highest of the three) on the extracellular fluid volume fraction is shown in Fig. 6, and on the extracellular Na^+ concentration is shown in Fig. 7. In a fashion analogous to the hyposmotic shock response, the cell regulation mechanisms again generate a propagating, albeit weaker, wave across the epidermis.

A comparison between the responses for all three potential differences at the position $x = 50$ μm is presented in Fig. 8. (For all ions, the greatest variations take place near the upper boundary, where zero mass flux is prescribed.) The simulation with the largest applied potential is also repeated with no cells inside the layer ($\theta_\beta = 0$ and $\theta_\alpha = 0.2$). Fig. 8a–c depicts the extracellular concentrations of Na^+, Cl^-, and K^+, for $\Delta\psi = -2.67$ mV, $\Delta\psi = -5.34$ mV and $\Delta\psi = -13.35$ mV. The impact of the electric field is greater on extracellular Na^+ concentration than on that for the Cl^- ions. The extracellular Na^+ concentration reaches a peak of more than twice its initial value, while the Cl^- concentration suffers a decrease as low as 30% of its initial magnitude. The comparison with the response of the layer devoid of cells (solid line) is particularly revealing. The impact that the transmembrane fluxes and cell volume

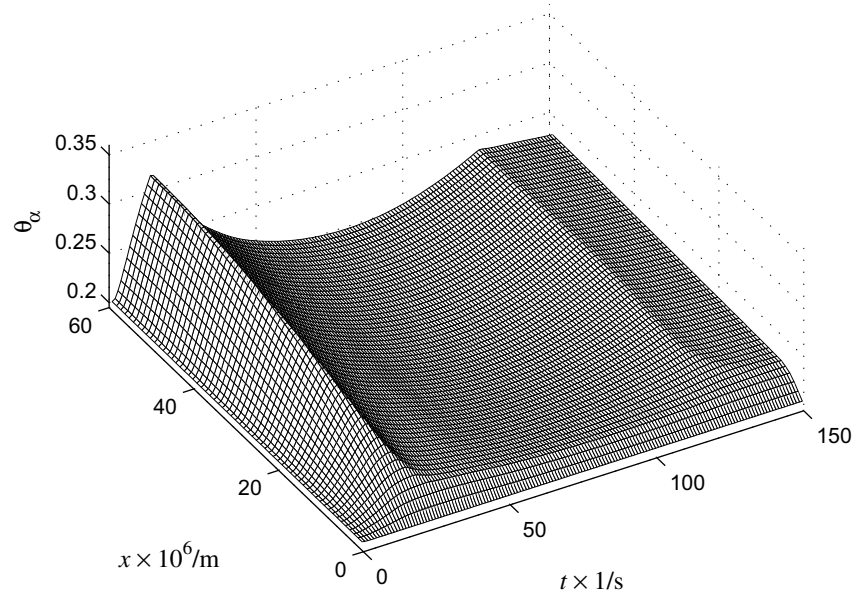

Fig. 6. Epidermis response with electromigration. Spatio-temporal variation of extracellular volume fraction for electric potential difference of 13.35 mV across 60 μm-thick tissue.

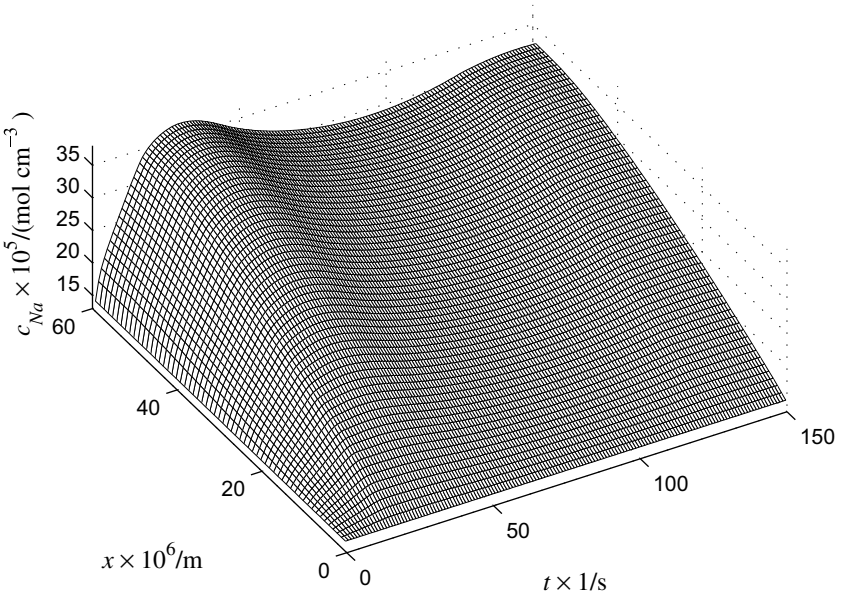

Fig. 7. Extracellular Na^+ concentration for electric potential difference of 13.35 mV across 60 μm-thick epidermis.

regulation have on ion extracellular concentrations for $\Delta\psi = -13.35$ mV can be seen by comparing the dash line with the solid line. Finally, the $Na^+ - K^+ -$ ATPase pump flux J_p (normalized by its initial value) is plotted in Fig. 8d. Noting that this property correlates with the intensity of the local cell activity, it is clear that the transmembrane pump flux increases with increasing potential difference. Consequently, the higher the potential difference, the faster is the active transport, and the stronger is the effect that the live cells have on the extracellular ion concentration profiles across the epidermis.

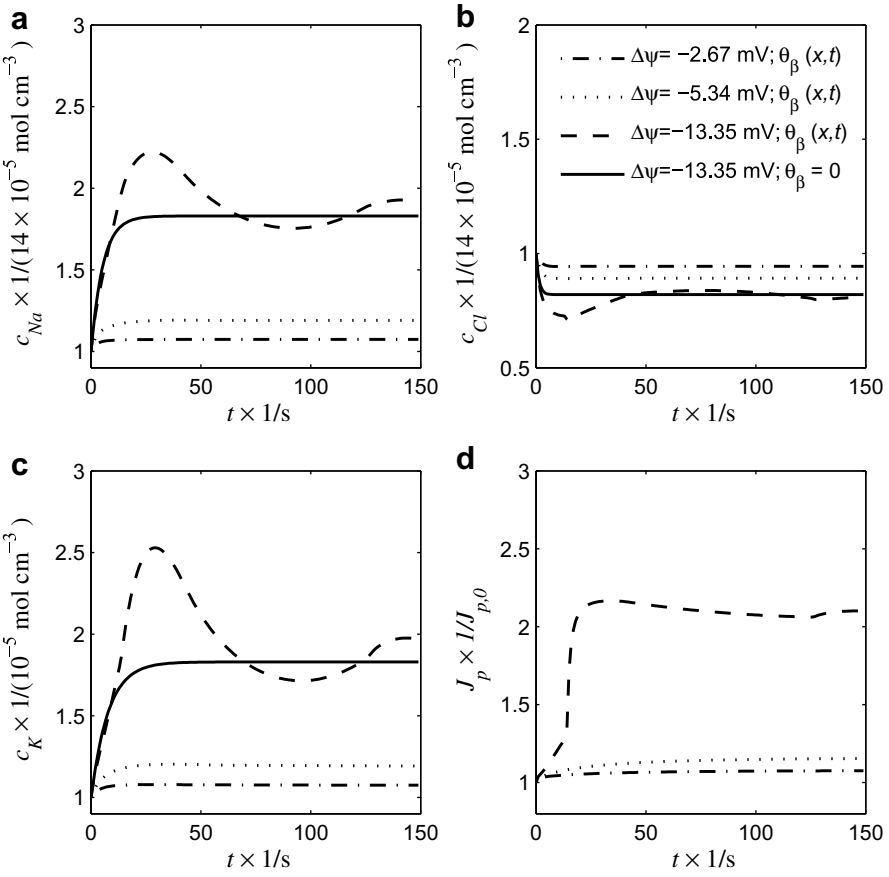

Fig. 8. Impact of imposed electric potential $\Delta\psi$ across 60μm-thick epidermis. Extracellular concentrations for (a) Na^+, (b) Cl^-, (c) K^+ and (d) cell transmembrane pump flux divided by its initial value. All plots correspond to position $x = 50$ μm.

4. Discussion

Motivated by the need to develop biophysically consistent models for transepidermal water transport, we have focused on modeling the redistribution of water and solutes in the human epidermis consisting of live swellable cells embedded in the tissue, and on the effect of transepidermal electric potential on this redistribution. We have employed a model of cell volume regulation available in the literature [13] to represent active transport through cells embedded in a non-deformable tissue. The active cell model is integrated with a passive biphasic transport model for extracellular transport. Electroneutrality is maintained in the intracellular and extracellular spaces since the combination of all passive and active fluxes carry the same amount of positive and negative charges across the cell membrane and the cells are modeled by point sink/sources.

The nonlinear response of the cell regulation mechanism becomes evident when the tissue is exposed to osmotic shocks imposed on one boundary. During the hyposmotic shock, the time delay component of the cell regulatory mechanism triggers propagating waves in the extracellular medium. Imposition of a hyposmotic shock for solutes Na^+ and Cl^- at one boundary of the extracellular region generates travelling waves in extracellular volume fraction and ion concentrations because the cells act alternatingly as mass sources and sinks. This is a result of the fact that cell volume regulation takes minutes (since it involves active solute transport which is slow) while osmotic equilibration occurs in seconds. A careful review of the literature has not revealed another report of this wave phenomenon. The onset of dispersive (wave-like) behavior in systems that are typically modeled by diffusive partial differential equations has an obvious mathematical appeal. The existence of wave like solutions of the model formulated here is characteristic of the class of excitable reaction-diffusion systems described by Grinrod [23]. If this phenomenon is observed experimentally, the generation of travelling waves in live tissue consisting of non-excitable cells might prove to serve an important physiological function which is as fascinating as that exhibited by excitable cells (neurons).

Another interesting finding is that imposing a negative electrostatic potential difference as small as $\Delta\psi = -13.35$ mV across a tissue layer of 60 μm thickness is enough to perturb the cell environment in a way similar to that predicted for a hyposmotic shock, namely, propagating waves appear in the medium. The imposition of an electric field of this magnitude or higher results in electromigration fluxes which are comparable to the ion diffusion flux. This apparently activates the same cell volume regulation mechanism as for the hyposmotic shock and results in wave-like behavior in ionic concentrations across the epidermis. Finally, by monitoring the transmembrane pump flux, we have found that maintaining a higher transepidermal potential requires faster active transport through the cells. This is consistent with the fact that higher gradients imply higher ionic fluxes, and these fluxes have to be balanced by the live cells which are trying to maintain internal equilibrium around certain set points.

By addressing the transport across a live tissue as a combination of mechanistic processes involving diffusion coupled to active transport through the cell phase, rather than simply treating tissues as passive or dead samples, the present work follows a physics-based path for the systematic study of all biomaterials. In the context of skin tissue modeling, many mechanisms involved in keratinocytes differentiation and adaptation to new environments are currently being discovered and explored, but complete cell regulation models are still unavailable. This work proposes a rational approach to modeling the redistribution of water and electrolytes in the epidermis, in terms of a mathematical model which is based on the fundamentals of continuum mechanics and mass transport and can additionally accommodate any improved models of epidermal cell regulation that will become available in the future.

5. Conclusions

This work reports the first -to our knowledge- local model for the redistribution of water and Na^+, K^+ and Cl^- ions in the epidermis which incorporates active transport through the live cells (keratinocytes) that comprise it. The molecular flux term contains both a diffusive and an electromigration flux component (given by the Nernst–Planck equation). Without the latter, imposition of a hyposmotic shock at one boundary of the extracellular region generates travelling waves in extracellular volume fraction and ion concentrations because the cells act alternatingly as mass sources and sinks. Imposing an electrostatic potential gradient $\Delta\psi$ across the epidermis, reveals a similar phenomenon. For small potential gradients (on the order of $(\Delta\psi)/(\Delta x) = 0.5$ mV/μm), the cell regulation mechanisms become sufficiently strong to perturb the extracellular profiles significantly. For example, the extracellular Na^+ concentration can deviate relative to that for the case without cells by up to of 50% of its initial value. Our results indicate that the cell regulation mechanisms have a strong impact on extracellular ion and water transport. Since the simplified model adopted here contains coupled ionic transport mechanisms (ion pumps and cotransporters), extracellular imbalances in certain ionic species perturbs other constituents. Consequently, active transport models have to be considered an indispensable element of live tissue models.

Acknowledgements

The work of C.F. was supported by the NSF Center of Advanced Materials for the Purification of Water with Systems (award CTS-0120978) and Coordenação de Aperfeiçoamento de Pessoal de Nivel Superior (Capes). J.G. thanks NIH (Grant HL090455-01) for financial support.

References

[1] B. Mudry, R.H. Guy, M.B. Delgado-Charro, Electromigration of ions across the skin: determination and prediction of transport numbers, J. Pharm. Sci. 95 (2006) 561–569.
[2] S. MacNeil, Progress and opportunities for tissue-engineered skin, Nature 445 (2007) 874–880.
[3] A.S. Verkman, More than just water channels: unexpected cellular roles of aquaporins, J. Cell Sci. 118 (2005) 3225–3232.
[4] M.A. Shannon, P. Bohn, M. Elimelech, J.G. Georgiadis, B. Marinas, A. Mayes, New science and technology for water purification in the coming decades, Nature 454 (2008) 331–341.
[5] P. Corcuff, F. Fiat, A.M. Minondo, Ultrastructure of the human stratum corneum, Skin Pharm. Appl. Skin Physiol. 14 (2001) 4–9.
[6] R.K. Freinkel, D.T. Woodley, The Biology of The Skin, The Parthenon Publishing Group, New York, USA, 2001.
[7] Y.N. Kalia, F. Pirot, R.H. Guy, Homogeneous transport in a heterogeneous membrane: water diffusion across human stratum corneum in vivo, Biophys. J. 71 (1996) 2692–2700.
[8] G.B. Kasting, N.D. Barai, T.-F. Wang, J.M. Nitsche, Mobility of water in human stratum corneum, J. Pharm. Sci. 92 (2003) 2326–2340.
[9] M. Denda, J. Hosoi, Y. Ashida, Visual imaging of ion distribution in human epidermis, Biochem. Biophys. Res. Commun. 272 (2000) 134–137.
[10] M. Denda, Y. Ashida, K. Inoue, N. Kumazawa, Skin surface electric potential induced by ion-flux through epidermal cell layers, Biochem. Biophys. Res. Commun. 284 (2001) 112–117.
[11] R. Glaser, Biophysics, Springer Verlag, Berlin, 2001.
[12] L. Reuss, B.H. Hirst, Water transport controversies – an overview, J. Physiol. 542.1 (2002) 1–2.
[13] J.A. Hernández, E. Cristina, Modeling cell volume regulation in nonexcitable cells: the roles of the Na^+ pump and of cotransport systems, Am. J. Physiol. 275 (1998) C1067–C1080.
[14] P.J. Caspers, G.W. Lucassen, G.J. Puppels, Combined in vivo confocal raman spectroscopy and confocal microscopy in human skin, Biophys. J. 85 (2003) 572–580.

[15] J.A. Hernández, J. Fischbarg, L.S. Liebovitch, Kinetic model of the effects of electrogenic enzymes on the membrane potential, J. Theor. Biol. 137 (1989) 113–125.
[16] J. Bear, J.M. Buchlin, Theory and Applications of Transport in Porous Media, Modelling and Applications of Transport Phenomena in Porous Media, Kluwer Academic Publishers, Netherlands, 1987.
[17] F.G. Helfferich, Ion Exchange, McGraw-Hill, 1962.
[18] W.Y. Gu, W.M. Lai, V.C. Mow, Transport of multi-electrolytes in charged hydrated biological soft tissues, Transport Porous Med. 34 (1999) 143–157.
[19] A.D. MacGillivray, Nernst–plank equations and the electroneutrality and donnan equilibrium assumptions, J. Chem. Phys. 48 (1968) 2903–2907.
[20] Y. Barrandon, H. Green, Cell size as determinant of the clone-forming ability of human keratinocytes, Proc. Nat. Acad. Sci. 82 (1985) 5390–5394.
[21] K.C. Chen, C. Nicholson, Changes in brain cell shape create residual extracellular space volume and explain tortuosity behavior during osmotic challenge, Proc. Nat. Acad. Sci. 97 (2000) 8306–8311.
[22] C.V. Falkenberg, Development and Verification of Poroelastic Barrier Model with Active Transport: Application in Human Epidermis. Ph.D Thesis, University of Illinois at Urbana-Champaign, USA, 2007.
[23] P. Grinrod, Patterns and Waves: the Theory and Applications of Reaction–Diffusion Equations, Clarendon Press, Oxford, 1991.
[24] S.W. Hui, Low voltage electroporation of the skin, or is it iontophoresis?, Biophys J. 74 (1998) 679–680.